Electrical behavior of memory devices based on fluorene-containing organic thin films

Panagiotis Dimitrakis,[1] Pascal Normand,[1] Dimitris Tsoukalas,[2] Christopher Pearson,[3] Jin H. Ahn,[3] Mohammed F. Mabrook,[3] Dagou A. Zeze,[3] Michael C. Petty,[3,a)] Kiran T. Kamtekar,[4] Changsheng Wang,[4] Martin R. Bryce,[4] and Mark Green[5]
[1]*National Centre for Scientific Research "Democritos," P.O. Box 60228, 15310 Aghia Paraskevi, Greece*
[2]*School of Applied Sciences, National Technical University of Athens, 15780 Zografou, Greece*
[3]*School of Engineering and Centre for Molecular and Nanoscale Electronics, Durham University, South Road, Durham DH1 3LE, United Kingdom*
[4]*Department of Chemistry and Centre for Molecular and Nanoscale Electronics, Durham University, South Road, Durham DH1 3LE, United Kingdom*
[5]*Physics Department, King's College London, Strand, London WC2R 2LS, United Kingdom*

(Received 16 May 2008; accepted 12 June 2008; published online 28 August 2008)

We report on switching and negative differential resistance (NDR) behaviors of crossed bar electrode structures based on Al/organic layer/Al devices in which the organic layer was a spin-coated layer of 7-{4-[5-(4-*tert*-butylphenyl)-1,3,4-oxadiazol-2-yl]phenyl}-9,9-dihexyl-*N*,*N*-diphenyl-fluoren-2-amine. The addition of gold nanoparticles (0.5 wt %) did not change the switching behavior of thicker film structures; however, devices incorporating the nanoparticles showed more reproducible characteristics. In most cases, a "forming" process, in which a large positive voltage was applied to the top Al electrode, was required before the NDR and conductivity switching were observed. Three different electrical conductivity mechanisms have been identified: Poole–Frenkel conductivity in unformed structures, linear current versus voltage characteristics for the ON state in formed devices, and superlinear current versus voltage behavior for the OFF state in formed devices. Models based on metallic filaments or on the injection and storage of charge do not explain all our experimental observations satisfactorily. Instead, an explanation based on the formation of nanocrystalline regions within the thin film is suggested. The devices can be used as two-terminal memory cells operating with unipolar voltage pulses. © *2008 American Institute of Physics*. [DOI: 10.1063/1.2968551]

I. INTRODUCTION

As progress in silicon microelectronics moves down the Moore's law curve to feature sizes below 50 nm, a worldwide research effort aiming at devices that go beyond conventional structures is underway. Memories represent by far the largest part of electronic systems, and there is a need to develop alternative architectures. Memories are either nonvolatile (for example, Flash memories) or volatile [e.g., dynamic random access memory (DRAM)]. An ideal device would combine the speed of DRAM, the retention characteristics of Flash structures, and the low cost, data density, and cycling endurance of hard-disk drives.

Beyond the 32 nm node, no consensus has emerged among device manufacturers on the nature of future memory structures.[1] Disruptive technologies that could be exploited include ferroelectric storage (ferroelectric RAM), magnetic storage (magnetoresistive RAM), and phase change materials (PCM memories). Such devices will be placed at the back end of commercial integrated circuits, with addressing and sensing circuits built into the silicon. Other memory structures have been considered in the International Technology Roadmap for Semiconductors.[2] Resistance change memories, in which the memory cell is defined by the area of two crossed metal lines, are very attractive as they are simple to fabricate (e.g., compared to transistor-based devices) and are highly scalable. This cross-point (or crossed-bar) architecture permits the closest packing of bit cells, with each occupying an area of $4F^2$, where F is the minimum feature size (the linewidth and spacing of the electrodes). Moreover, if the "active" material can be deposited at low temperature, such devices could be stacked in three dimensions as additional processing to form an additional memory layer will not affect the underlying layer(s).

Over the past 40 years, there have been many reports of switching and memory effects in thin films.[3] The film thicknesses are generally less than 1 μm, and the phenomena are observed in different types of materials (inorganic compounds, such as silicon dioxide, and organic compounds, such as polymers and charge-transfer complexes). Furthermore, the thin films have been formed using a variety of techniques (e.g., spin coating and thermal evaporation). The only experimental parameter that is common to all the structures studied is the presence of metallic electrodes (e.g., Al) below and on top of the thin film. A significant development is a recent publication describing a 160 kbit memory based on a bistable rotaxane.[4]

There is currently no agreement on how the thin film memories operate. Indeed, a number of different categories of devices have been identified according to their switching behavior.[3] Many of the recipes for switching are based on the

a)Electronic mail: m.c.petty@durham.ac.uk.

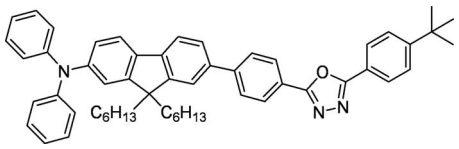

FIG. 1. Chemical structure of compound **1**, 7-{4-[5-(4-*tert*-butylphenyl)-1,3,4-oxadiazol-2-yl]phenyl}-9,9-dihexyl-*N*,*N*-diphenyl-fluoren-2-amine used in this study.

incorporation of metallic nanoparticles within an organic thin film.[5–7] The presence of the nanoparticles is thought to influence the transfer of charge (e.g., by a trapping/hopping process).[1] However, switching has also been reported in devices in which a single organic layer is sandwiched between metallic electrodes.[3,8,9] Bistable devices that do not include nanoparticles are preferable as their presence will restrict the device scaling, i.e., when the cell dimensions become comparable to those of the nanoparticles. In previous work, we have described bistable switching and memory effects in a single fluorene-containing organic compound sandwiched between aluminum electrodes.[10,11] Here, we report, in more detail, on the electrical characteristics of such devices in an attempt to identify the key conduction processes and to elucidate the device operation. We also compare the behavior of structures with incorporated metallic nanoparticles to those based on a single material.

II. EXPERIMENT

The chemical structure of the compound used in this study, compound **1**,7-{4-[5-(4-*tert*-butylphenyl)-1,3,4-oxadiazol-2-yl]phenyl}-9,9-dihexyl-*N*,*N*-diphenyl-fluoren-2-amine is depicted in Fig. 1; the material was synthesized as described previously and has been used in the fabrication of organic light-emitting devices.[12] The compound is a triad molecule: the oxadiazole, triarylamine, and fluorene units serve as the electron transport, hole transport, and emitter segments of the molecule. The organically capped nanoparticles used in this work (Q-Au) were prepared using Schlenk line techniques.[13,14]

The devices investigated in this work were all prepared in a class 1000 microelectronics clean room. Substrates were glass microscope slides. These were scrupulously cleaned using the following procedure: (i) rinse in a stream of propan-2-ol from a washbottle, (ii) sonicate in propan-2-ol for 15 min, (iii) rinse in a stream of propan-2-ol from a washbottle, (iv) dry in a stream of nitrogen gas, (v) rinse in a stream of acetone from a washbottle, (vi) sonicate in acetone for 15 min, (vii) rinse in a stream of acetone from a washbottle, (viii) dry in a stream of nitrogen gas, (ix) rinse in a stream of ultrapure water, (x) sonicate in 2% aqueous Decon 90 solution for 15 min, (xi) rinse in a stream of ultrapure water, (xii) sonicate in ultrapure water for 15 min, (xiii) rinse in a stream of ultrapure water, and (xiv) dry in a stream of nitrogen gas.

The bottom electrodes, consisting of 100 nm thick strips of aluminum 1.5 mm wide and 1.5 mm apart, were deposited by thermal evaporation through a shadow mask at a rate of 0.5 ± 0.1 nm s^{-1} under a vacuum of approximately 5×10^{-6} mbar. Following metallization, the slides were cut into pieces 2 cm long. The active organic layer was deposited by spin coating in a glove box under a nitrogen atmosphere. A solution of compound **1** was prepared by adding 1 ml of Aristar Grade chloroform to the solid to give a concentration of 6.70 g l^{-1}. For solutions containing Q-Au nanoparticles, 6.6 mg of the active material was dissolved in 0.83 ml of chloroform, and 0.17 ml of a 0.2 g l^{-1} chloroform solution of Q-Au was added to give a solution of 0.5 wt % of nanoparticles. The spin casting parameters for Q-Au doped films were the same as those for the pure material: 300 μl of solution was applied to the surface of the substrate using a pipette, so that the surface was completely covered. The spinner motor was immediately switched on at 1000 rpm for a fixed time (nominally 60 s to provide a 50 nm thick film).

To complete the devices, 100 nm thick aluminum strips, perpendicular to and having the same dimensions as the bottom electrodes, were thermally evaporated on top of the organic layers. The evaporation conditions were the same as those used for the bottom electrodes. The thickness of the organic layers was measured by mechanically removing the film (by abrasion in an area between the metal electrodes) and then imaging the step created using a Digital Instruments NanoMan atomic force microscope in the tapping mode.

An electrical characterization of the devices was undertaken with the samples in vacuum and using a Keithley 2400 sourcemeter. The admittance of the devices over a frequency range of 10 Hz to 1 MHz was monitored with an *LCR* bridge (HP4192); the capacitance at 1 MHz was also measured with a Boonton capacitance meter. Rigorous and systematic testing procedures were adopted to check for reproducibility and in order to make valid comparisons between different devices. Two contrasting measurement procedures were adopted. These are referred to as measurement schemes A and B, and are described, in some detail, below.

A. Measurement scheme A: Unipolar voltage sweep

Start with a new (virgin) device and attach the "Hi" terminal of the voltage source to the top electrode.

(1) Perform sequentially the following voltage sweeps (voltage step of 0.1 V, step delay time of 1 s): $0 \rightarrow +1$ V, $0 \rightarrow +2$ V, $0 \rightarrow +3$ V, ..., $0 \rightarrow +7$ V (positive voltage applied to the Al top electrode) looking for negative differential resistance (NDR) in the measured current I versus voltage V curves or "conduction" switching from a low state to a high state.
(2) If NDR was not observed, then the voltage sweep $0 \rightarrow +7$ V was repeated a few more times to see if the NDR region appeared. For some devices, scans were also made to higher voltages.

If NDR was observed, then voltage pulses were applied in order to investigate the memory characteristics of the device under test. The pulse height was equal to the voltage corresponding to the current maximum (before the onset of the NDR region) in order to switch the device into the high conduction state ("write" memory operation), while the gate voltage corresponding to the lowest current value in the

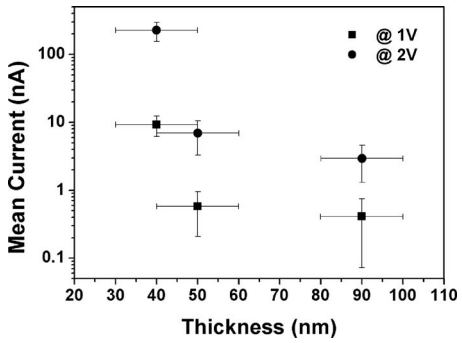

FIG. 2. Current through a new Al/compound **1**/Al device as a function of organic layer thickness for two applied dc voltages.

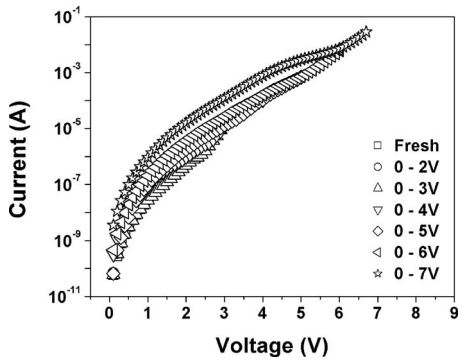

FIG. 3. Current vs voltage characteristics for a new Al/40 nm compound **1**/Al device. Measurements taken by scanning to progressively higher voltages (measurement scheme A: unipolar voltage sweep).

NDR region was chosen as the pulse height to drive the device into the low conduction state ("erase" memory operation).

B. Measurement scheme B: Bipolar voltage sweep

Start with a new device and attach the Hi terminal of the voltage source to the top electrode.

(1) Sweep the voltage in the range $-8\ \text{V} \rightarrow +8\ \text{V} \rightarrow -8\ \text{V}$ (negative voltage initially applied to the Al top electrode). Data shown as *I-Va* (normal mode).
(2) Repeat step (1). Data shown as *I-Vb*.
(3) Reverse polarity of the connections from the voltage source and perform the same voltage sweep $-8\ \text{V} \rightarrow +8\ \text{V} \rightarrow -8\ \text{V}$ (positive voltage initially applied to the top Al electrode). Data shown as *I-Vc*.
(4) Select a new device and connect the voltage "Lo" terminal to the top electrode.
(5) Repeat steps (1)–(3). Data shown as *RI-Va*, *RI-Vb*, and *RI-Vc* (reverse mode).

Measurement scheme A invariably revealed the devices in their low conductivity (OFF) state, whereas the measurement scheme B procedure usually showed the devices in their high conductivity (ON) state; voltage pulsing was needed to achieve the low conductivity OFF state.

III. RESULTS

A. Devices without nanoparticles: Measurement scheme A

Figure 2 shows the variation of current with the organic film thickness for Al/compound **1**/Al structures for applied voltages of 1 and 2 V. The data are for new devices, and the error bars reflect the standard errors for measurements on 6–11 different samples. The decrease in current with increasing film thickness (note the logarithmic current scale) suggests that a significant part of the applied voltage is dropped across the organic layer (i.e., as opposed to the interfacial "oxide" regions).

The current versus voltage data obtained following measurement procedure A are shown in Fig. 3 for devices containing 40 nm of compound **1**. Scans to progressively higher voltages produced current versus voltage curves displaced to higher currents. This might result from some sort of annealing of the film and/or contacts. However, no anomalous regions (e.g., switching or NDR) were observed with applied voltages up to the maximum used (7 V).

We have considered that the presence of Schottky barriers between the aluminum electrodes and the organic thin film might account for the current versus voltage behavior shown in Fig. 3. For any applied voltage, the conductivity would be determined by the junction that was reverse biased, resulting in a low current with a very weak dependence on the voltage. This is not observed in Fig. 3. We have also measured devices in which the Al bottom electrode was replaced by indium tin oxide (a high work function material); these showed a similar current versus voltage behavior to that of the Al/compound **1**/Al structures. Consequently, we suggest that Schottky barriers are not significant in our devices.

A number of other dc electronic conduction mechanisms might be expected in thin organic films.[15–17] These include direct quantum mechanical tunneling, space-charge-limited conductivity, Schottky emission, Poole–Frenkel conductivity, and Fowler–Nordheim tunneling. The organic layers used in this work are too thick (all >30 nm) to expect direct quantum mechanical tunneling between the metallic electrodes. However, tunneling may occur between defect sites if these are sufficiently close together. For low applied voltages (less than the energy barrier height divided by the electronic charge), the expected dependence of current density J on applied voltage will be

$$J \propto V. \tag{1}$$

However, at higher voltages, the J-V relationship can deviate from linearity. For example, one theoretically predicted current density versus voltage dependence for a symmetrical rectangular barrier takes the form[18]

$$J \propto \exp(-BV^2)\sinh\left(\frac{CV}{2}\right), \tag{2}$$

where B and C are coefficients related to the tunneling barrier height.

For conditions (super-Ohmic contacts) where the current is only limited by the space charge between the electrodes,

space-charge-limited conductivity (SCLC) may be observed. In this case, the relationship between J and V is given by a power law

$$J \propto L\left(\frac{V}{L^2}\right)^n, \tag{3}$$

where L is the distance between the electrodes and n is an integer. For single carrier injection (electrons or holes) $n=2$, whereas for double carrier injection (electrons and holes) $n=3$.

At high electric fields, Schottky emission or Poole–Frenkel conduction may occur. These effects result from the reduction in the potential barrier to carriers by the electric field at either the surface (Schottky effect) or surrounding bulk impurities (Poole–Frenkel conduction). The current density versus voltage behavior for Schottky emission is given by

$$J \propto \exp(aV^{1/2}), \tag{4}$$

whereas the corresponding equation for Poole–Frenkel conduction is

$$J \propto V \exp(bV^{1/2}). \tag{5}$$

In both cases, a and b are constants.

Fowler–Nordheim conduction occurs if the electric field at the electrode is sufficiently large to allow carriers to tunnel from the metal (through the potential barrier) to the conduction band of the insulator. The dependence of current density on voltage is now

$$J \propto V^2 \exp\left(\frac{-c}{V}\right), \tag{6}$$

where c is a further constant.

The experimental results in Fig. 3 suggest a nonlinear relationship between the current and the applied voltage. Figures 4(a)–4(c) show attempts to fit these data to the Poole–Frenkel [Fig. 4(a)], Fowler-Nordheim [Fig. 4(b)], and SCLC models [Fig. 4(c)]. The only conduction process showing a reasonable fit to the theory is Poole–Frenkel conductivity, for which Fig. 4(a) shows good straight lines in the $\log(I/V)$ versus $V^{1/2}$ plots over several orders of magnitude of current. We have also attempted to fit the experimental data to the expression for Schottky emission [Eq. (4)]. However, the fits were significantly inferior to those for Poole–Frenkel conduction [Eq. (5)].

The constant b in Eq. (5) is given by[15]

$$b = \frac{1}{kT}\left(\frac{e^3}{d\pi\varepsilon\varepsilon_0}\right)^{1/2}, \tag{7}$$

where d is the film thickness, T is the temperature, e is the electronic charge, k is Boltzmann constant, ε_0 is the permittivity of free space, and ε is the relative permittivity of the organic film. By fitting straight lines to the data in Fig. 4(a), relative permittivities in the range of 6–8 are obtained. These values seem high. Measurements of the capacitance (at 1 MHz) of one of our devices (with no incorporated Q-Au) revealed a relative permittivity of 3.6. Spin-coated layers of related polyfluorene compounds have been found to possess

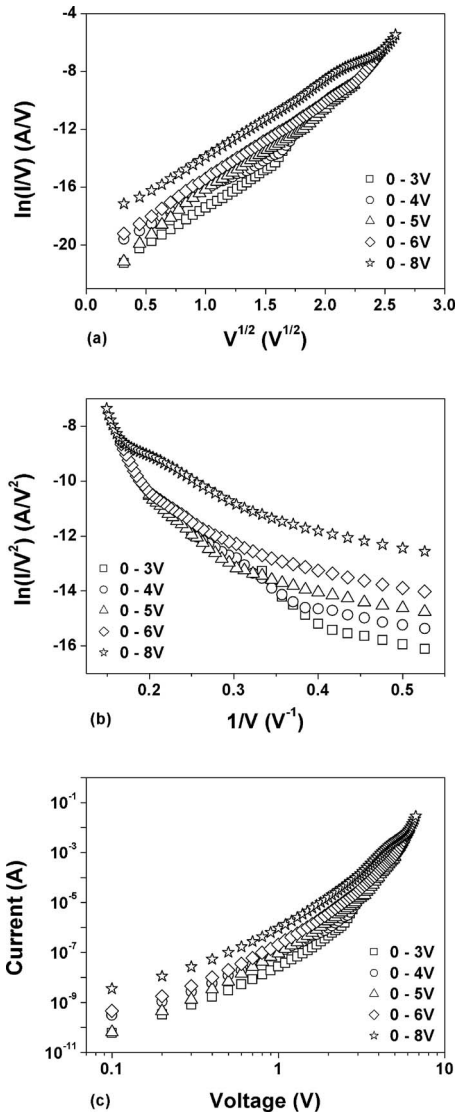

FIG. 4. (a) Electrical data in Fig. 3 plotted in the form $\ln(I/V)$ versus $V^{1/2}$. (b) Electrical data in Fig. 3 plotted in the form $\ln(I/V^2)$ vs V^{-1}. (c) Electrical data in Fig. 3 plotted in the form $\ln(I)$ vs $\log(V)$.

a relative permittivity of approximately 2.7 at a frequency of 10 kHz.[19] The discrepancy between our experimental and theoretical values of permittivity could well be the result of an inaccurate value for the film thickness or could reflect some deviation from the simple Poole–Frenkel theory.[15] The presence of a thin layer of aluminum oxide on the aluminum electrode(s) (with a relative permittivity of approximately 9) will also reduce the electric field in the organic film, complicating the above analysis.

Increasing the thickness of the organic film revealed both switching and NDR effects. Figure 5 shows the current versus voltage behavior for an Al/50 nm compound **1**/Al structure measured under scans to progressively higher voltages (measurement scheme A). The scan to 8 V shows some switching behavior, while a NDR region is revealed with a voltage scan to 10 V. There is clearly some kind of device "formation" process. This process only occurred with a positive potential applied to the top electrode. The current versus voltage characteristics for a fully formed device are depicted in Fig. 6. The ON (high conductivity) and OFF (low conduc-

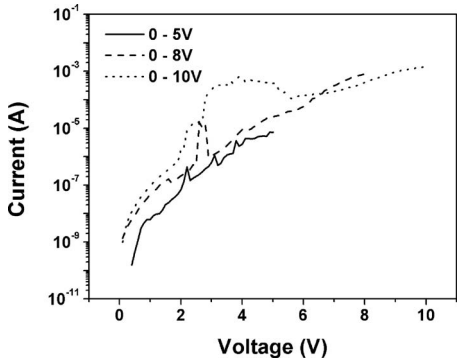

FIG. 5. Current vs voltage characteristics for a new Al/50 nm compound **1**/Al device. Measurements taken by scanning to progressively higher voltages (measurement scheme A: unipolar voltage sweep).

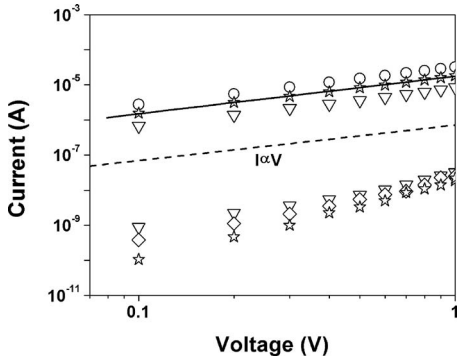

FIG. 7. Log(current) vs log(voltage) data for Al/90 nm compound **1**/Al in the OFF (lower set of curves) and ON states after application of +3 V/5 s write pulses and +6 V/5 s erase pulses.

tivity) states are evident. Once formed, these characteristics were independent of the polarity of the applied voltage. The NDR and memory effects are very similar to those reported by Bozano *et al.*[5] for three-layer devices in which an aluminum layer was sandwiched between thin films of aluminum tris(8-hydroxyquinoline) (Alq_3). Such characteristics should be distinguished from those reports in which bistable switching is observed, but the NDR region is absent.[3,7,9,20]

The ON state was obtained by applying a voltage close to the current maximum (just before the NDR region) and by reducing it rapidly to zero. In contrast, switching from the high conductivity ON state to the OFF sate was accomplished by selecting a voltage near that corresponding to the current minimum in the NDR region and reducing this rapidly to zero (erase). The state of the device (ON or OFF) could be determined by measuring the current at a voltage of 1 V (read).

We have undertaken a preliminary study of the admittance of our devices over the range of 10 Hz to 1 MHz in both the ON and OFF states. The results (to be presented elsewhere) are in broad agreement with those of Cölle and co-workers.[24,25] The equivalent circuit of our device in both states can be represented by a parallel combination of a capacitor (the geometrical capacitance of the device) and a resistor, together with a small series resistance ($<10\ \Omega$) representing the resistance of the contacts and connections. The switching only affects the device resistance, and there is no evidence of charge injection into the bulk of the organic thin film.

Figure 7 shows the log(current) versus log(voltage) characteristics of both the ON and OFF states for a Al/90 nm compound **1**/Al structure, with applied voltages up to 1 V. The high and low states were obtained after application of a +3 V, 5 s write pulse and a +6 V, 5 s erase pulse, respectively. The ON state conductivity seems to be well described by an $I \propto V$ relationship, perhaps reflecting an Ohmic or a tunneling process. In contrast, the current versus voltage curves in the OFF state are nonlinear. These can be fitted approximately with a power law of the form $I \propto V^n$ with $1.5 < n < 2.2$; however, these fits are far from perfect. The conduction processes for both the ON and OFF states are clearly different from the Poole–Frenkel mechanism identified for the structures containing the 40 nm thick organic film [Fig. 4(a)].

B. Devices with nanoparticles: Measurement scheme A

Similar experiments to those described in the previous section were then undertaken using samples containing 0.5% of the gold nanoparticles. The average currents versus organic film thickness at two different applied voltages are shown in Fig. 8. The error bars represent the standard errors on four to six different samples. These data can be contrasted with those in Fig. 2 for the equivalent devices with no incorporated nanoparticles. Within experimental error, both sets of

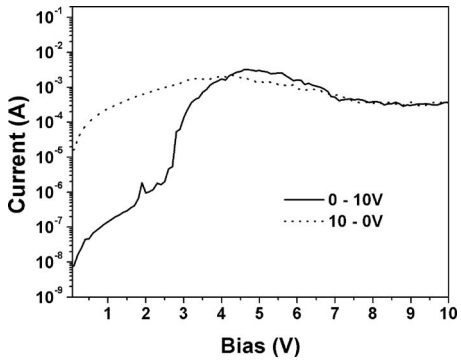

FIG. 6. Current vs voltage characteristics of an Al/50 nm compound **1**/Al device following the formation process. Voltage scan from 0 to +10 V (on the top electrode) (full line) and +10 to 0 V (dotted line).

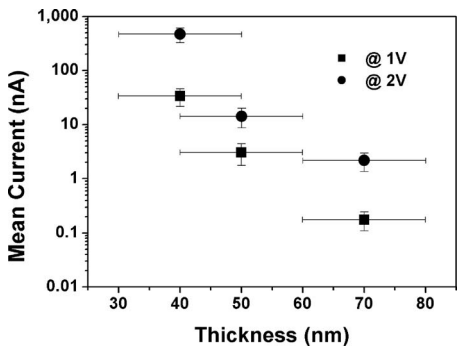

FIG. 8. Current through a new Al/compound **1**+0.5% Q-Au/Al device as a function of organic layer thickness for two applied dc voltages.

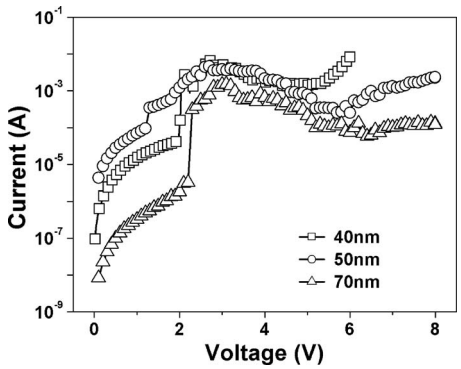

FIG. 9. Current vs voltage characteristics for Al/compound **1**+0.5% Q-Au/Al structures following device formation. The different curves correspond to different organic film thicknesses.

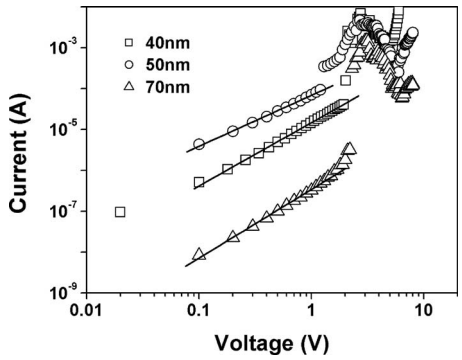

FIG. 11. Log(current) vs log(voltage) for Al/compound **1**+0.5% Q-Au/Al structures in their OFF states. The different curves correspond to different thicknesses of the organic film.

data are very similar, although it might be argued that the currents through the Q-Au-containing devices are somewhat larger at lower film thicknesses.

All the Q-Au-containing structures investigated exhibited NDR and switching effects, irrespective of the thickness of the organic layer. In most cases, a formation procedure (positive voltage applied to the top aluminum electrode) was needed before these conductivity phenomena were observed. However, some of the thicker structures (70 nm organic film thickness) exhibited NDR and switching behaviors on the first voltage scan. Generally, the electrical characteristics of the nanoparticle-containing devices were less noisy and more reproducible than those measured on devices with no Q-Au. The effects of different organic film thicknesses on the electrical characteristics of the Q-Au-containing devices are shown in Fig. 9. The current maximum, at approximately 3 V, is similar in all the samples studied. However, the minimum value (i.e., the current valley) appears to increase with the sample thickness. The best switching, in terms of the largest peak-to-valley ratio, was achieved with the thickest (70 nm) sample. This is shown in Fig. 10, which depicts the read current, I_{read} (measured at an applied voltage of 1 V), following write and erase pulses for different thickness samples incorporating the Q-Au nanoparticles.

The current versus voltage data presented in Fig. 9 are redrawn in the form of log(current) versus log(voltage) in Fig. 11. The OFF state current is characterized approximately by a power law, similar to the data for the devices with no Q-Au (Fig. 7). In the case of the nanoparticle-containing devices, the value of n is then in the range of 1.2–1.7.

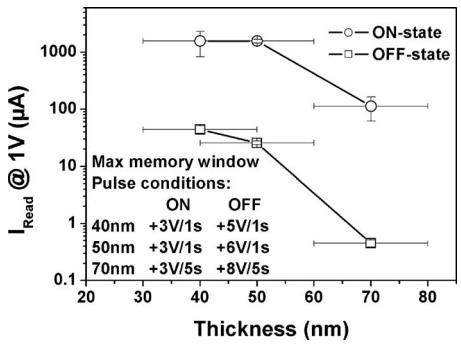

FIG. 10. Read current (at 1 V) following write and erase pulses for Al/compound **1**+0.5% Q-Au/Al structures as a function of the thickness of the organic film.

C. Measurement scheme B

Voltage scans from −8 to +8 V, as described in Sec. II, for 40 nm thick samples with no Q-Au are shown in Fig. 12. In Fig. 12(a) the first two curves, *I-Va* and *I-Vb*, represent consecutive scans on a new sample, while the curve denoted by *I-Vc* is a subsequent scan, with the voltage polarity reversed. If the voltage polarity applied to a fresh sample is in the opposite sense, this generates curves *RI-Va*, *RI-Vb*, and *RI-Vc*, shown in Fig. 12(b). In all these measurement configurations, neither NDR nor switching was observed in the 40 nm samples. Apart from the slightly higher current noted

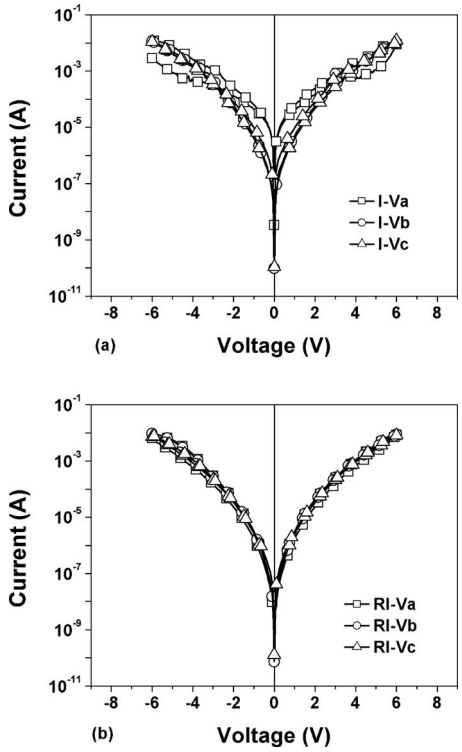

FIG. 12. Current vs voltage characteristics for an Al/40 nm compound **1**/Al structure. Measurement scheme B (bipolar voltage sweep). (a) Normal scans. (b) Reverse mode scans.

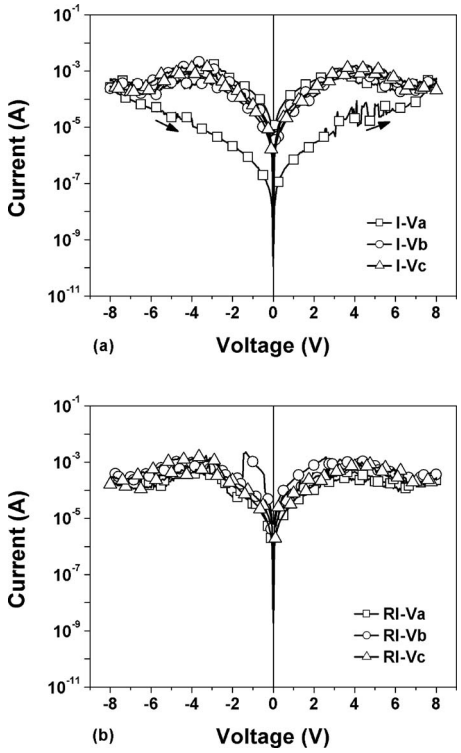

FIG. 13. Current vs voltage characteristics for an Al/50 nm compound **1**/Al structure. Measurement scheme B (bipolar voltage sweep). (a) Normal scans. (b) Reverse scans.

for the initial scan in the normal polarity (curve *I-Va*), the curves are more or less identical and can be fitted very well to the Poole–Frenkel model given by Eq. (5).

Electrical data for devices with a 50 nm organic layer are shown in Fig. 13. In this case NDR is clearly evident. However, the appearance of this phenomenon is dependent on the precise sequence of the measurements. For example, in the case of the first −8 to +8 V scan in the normal mode, Fig. 13(a) (curve *I-Va*) does not reveal the NDR. This only appears in the +8 to −8 V sweep, i.e., after a positive voltage has been applied to the top Al electrode. In contrast, if +8 V is applied to a fresh device—Fig. 13(b) curve *RI-Va*—the NDR region is immediately present. These data are entirely consistent with the observation in the previous sections (measurement scheme A) that a positive voltage needed to be applied to the top electrode in order to "form" the device.

Measurement scheme B invariably revealed the devices in their high conductivity ON state. Following the device formation, continuous voltage scanning between −8 and +8 V always resulted in curves of the type depicted in Fig. 13(b). To reveal the OFF state, the applied voltage was first fixed at the point corresponding to the current minimum in the NDR region and then rapidly reduced to zero. This switching would occur using either a positive or a negative voltage, i.e., following formation, the device was completely symmetrical, as suggested by the current versus voltage data in Fig. 13(b).

Similar results were obtained for samples containing the Q-Au nanoparticles. In these cases, a forming process (positive voltage applied to the top Al contact) was generally

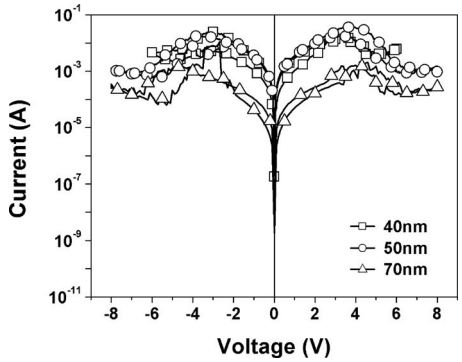

FIG. 14. Current vs voltage characteristics, measurement scheme B (bipolar voltage sweep), initial reverse scans, for Al/compound **1**+0.5% Q-Au/Al structures. The different curves correspond to different organic film thicknesses.

needed, although, as noted in the previous section, some of the thicker Q-Au-containing devices did not require forming. Figure 14 shows the initial reverse scans (*RI-Va* measurements) for three different thickness structures incorporating Q-Au. All the devices reveal NDR regions. The current values are smaller for the thickest (70 nm) device, which reveals some noise ("switching"). The current maxima for the Q-Au-containing devices are higher than the corresponding devices without nanoparticles (compare the absolute current levels for the 50 nm Q-Au structure in Fig. 14 to those shown in Fig. 13).

It was found to be possible to "unform" (in contrast to switching to the OFF state) some of the devices with a negative voltage applied to the top Al electrode. For example, Fig. 15 shows results for an Al/50 nm compound **1**+0.5%

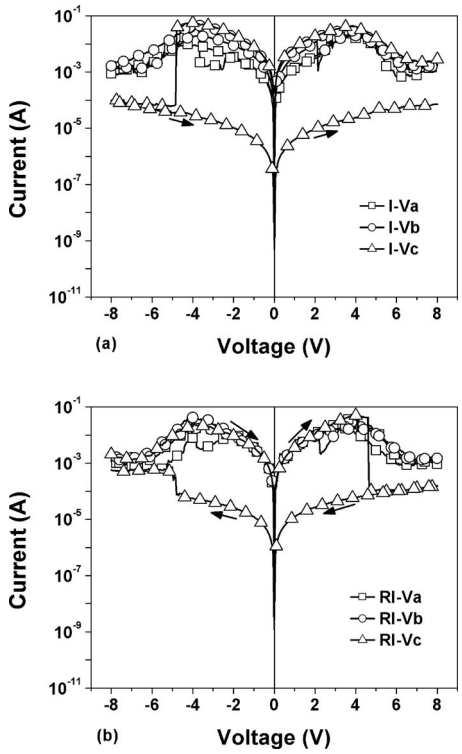

FIG. 15. Current vs voltage characteristics for Al/50 nm compound **1** +0.5% Q-Au/Al structure. Measurement scheme B (bipolar voltage sweep). (a) Normal scans. (b) Reverse scans.

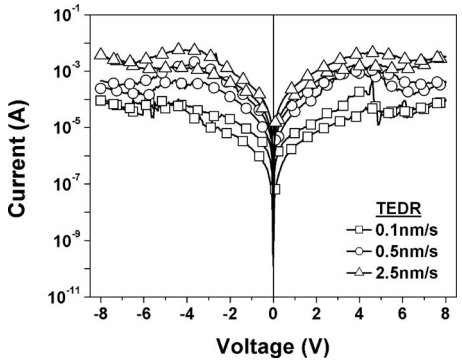

FIG. 16. Effect of the top electrode deposition rate (TEDR) on the current vs voltage characteristics for Al/50 nm compound **1**/Al structures. Second scans in the normal mode. Measurement scheme B (bipolar voltage sweep).

Q-Au/Al structure. The normal mode scans [Fig. 15(a)] reveal the elimination of the NDR region on the application of a negative bias to the top electrode (*I-Vc* scan), while the reverse mode scans [Fig. 15(b)] show the elimination of the NDR region with a negative applied voltage to the top electrode and its reappearance later in the same scan with a positive voltage applied to the top aluminum electrode (*RI-Vc* scan).

D. Effect of top electrode deposition rate

In a series of experiments, we have investigated the effect of the deposition rate of the top electrode on the electrical behavior of the devices (keeping the overall top electrode thickness the same). For the experiments described in the previous section, the aluminum top electrode was deposited at 0.5 nm s^{-1}. Here, we have used both higher (2.5 nm s^{-1}) and lower (0.1 nm s^{-1}) rates. Figure 16 shows the current versus voltage curves for 50 nm devices with no Q-Au. These data were recorded using measurement scheme B, and the data depicted are for the second scans in the normal mode, corresponding to *I-Vb*. Therefore, these measurements are made following the device formation process. It is evident that a relatively slow evaporation of aluminum results in a device with a weak NDR region. Data for 50 nm Q-Au-containing structures are shown in Fig. 17 for normal scans *I-Vb*; Fig. 17(a) shows the data on a log(current) scale, while Fig. 17(b) is for the same data on a linear current scale. Once again, the slowest deposition rate gives the weakest NDR.

We have also attempted to study the effect of the bottom aluminum electrode on the device characteristics. By preparing the devices in a nitrogen glove box (in which the Al evaporator was installed), we hoped to minimize the thickness of the aluminum oxide layer beneath the spin-coated organic film. Structures with and without the Q-Au nanoparticles were investigated. This fabrication procedure led either to devices that did not exhibit any switching or to devices that showed a very noisy switching behavior. Our conclusion, therefore, was that the presence of a native aluminum oxide on the bottom electrode was crucial for reproducible NDR and switching effects.

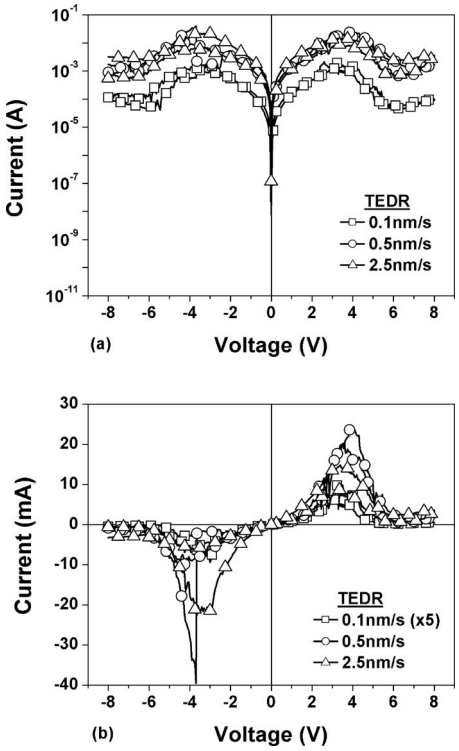

FIG. 17. Effect of TEDR on the current vs voltage characteristics for Al/50 nm compound **1**+0.5% Q-Au/Al structures. Measurement scheme B (bipolar voltage sweep). Initial scan in the normal mode. (a) Semilogarithmic scale. (b) Linear scale.

IV. DISCUSSION

The results from our various experiments presented here can be summarized as follows:

(a) Switching and NDR can be observed in Al/compound **1**/Al structures in which the organic film thickness is greater than about 50 nm. The addition of gold nanoparticles (0.5 wt %) does not change the basic switching behavior; however, devices incorporating the nanoparticles show more reproducible characteristics.

(b) Samples in which the organic film is less than about 50 nm in thickness do not exhibit NDR or switching unless a small concentration of gold nanoparticles is added.

(c) A device formation process, requiring the application of a positive voltage to the top Al electrode, is generally needed before the NDR and switching become evident.

(d) The presence of an oxide layer on the bottom aluminum electrode is necessary for reproducible NDR and switching.

(e) A number of different electrical conductivity processes have been identified: Poole–Frenkel conductivity in unformed structures, linear current versus voltage characteristics for the ON state for formed devices, and superlinear current versus voltage behavior for the OFF state in formed devices.

Any theory to explain the switching and NDR behaviors in resistive thin film memory devices must account for all the experimental observations. Currently, the explanations for

these phenomena fall into two distinct categories: (i) the injection and storage of charge in the thin film and (ii) metallic filament formation. The formation process must hold a strong clue to the operating mechanism of our devices. Other workers have also noted that some kind of formation is required before switching effects are observed, but sometimes details of the process are sketchy. There is also some confusion in the literature between the electrical behavior of the unformed (virgin) device and that of the ON and OFF states. In common with the recent data reported by Cölle and co-workers[24,25] for aluminum/organic layer/metal devices, we have found *three* different states for our devices, each exhibiting different current versus voltage behaviors: unformed, formed ON state, and formed OFF state.

Very similar electrical data to those presented here were also reported in 1967 by Simmons and Verderber.[21] These authors used thin (20–300 nm) films of silicon oxide sandwiched between aluminum and gold electrodes. The forming process (described in detail by the authors) involved the application of a positive voltage to the gold electrode. This was thought to result in Au ions being injected into the insulating film. However, subsequent experiments by Dearnaley *et al.*[22] contradicted this idea. A theory was developed in terms of the growth and thermal rupture of many conducting filaments through the insulating layer. Further different mechanisms were proposed by the same authors to explain the formation.[23] In the work of Cölle and co-workers,[24,25] it is argued that the device formation results from a "soft" breakdown in the underlying aluminum oxide layer. The role of the organic film in the subsequent switching is only as a limiting series resistance.

Our current experiments also reveal that the electrical behavior of our devices depends on the evaporation conditions of the top metal electrode. The interaction of vapor-deposited metal atoms with some organic materials has been reported. In the case of self-assembled monolayers, it was observed that Al atoms exhibit a wide range of chemical and physical interactions.[26,27] For example, reactive surfaces, such as -COOH and -OH, can interact with the aluminum to form a series of organometallic complexes in the first few monolayers. In contrast, when the terminal group of the alkyl chain of the self-assembled monolayer contains an unreactive group, such as $-CH_3$, penetration of the metal atoms through the monolayer occurs to the Au/S interface where it forms an adsorbed layer. Once the formation of this layer is complete, the monolayer penetration ceases and the aluminum overlayer begins to grow at the self-assembled monolayer/vacuum interface. On this basis, we would expect the Al to bond strongly to the various polar groups of compound **1** and not to penetrate the thin film appreciably. The nature of the thin organometallic region that forms will almost certainly depend on the metal evaporation conditions, such as the evaporation rate. The molecules in our spin-coated film may not be as highly packed as the alkyl chains in a self-assembled monolayer, and 50 nm films of compound **1** are likely to contain defects.

Tang *et al.* suggested that evaporating metals can form metal islands within nanometer-wide crevices in organic thin films.[28] Our devices are electrically resistive in their as-deposited state, with no evidence of metallic filament formation. If metal filaments are responsible for the switching and memory effects in our devices, then these must result from the formation process. Any filaments must also be destroyed by switching the device to its OFF state. In two exploratory experiments, we have modified the top electrode in our devices: (i) by evaporating a thin (1.8 nm) layer of Cr beneath the Al and (ii) by depositing either two or four Langmuir–Blodgett (LB) layers of arachidic acid or cadmium arachidate between the spin-coated organic layer and the Al top electrode. Both these changes would have been expected to influence the diffusion of Al from the top electrode into the spin-coated film. For example, an ultrathin (submonolayer) chromium film has been shown to be a very effective barrier against the penetration of Ag into organic films.[29] However, devices with modified top electrodes exhibited NDR and switching effects that were very similar to the reference structures.

The current versus voltage behavior of our unformed structures can be explained very well by Poole–Frenkel conductivity. The ON state of the formed device exhibits an approximately linear dependence of the current on the applied voltage. This may be the Ohmic conductivity associated with conductive metal filaments or tunneling through defect states in the organic film, as suggested by Simmons and Verderber.[21] The OFF state conductivity shows a roughly quadratic dependence of current upon voltage. This behavior is reminiscent of single carrier space-charge injection [Eq. (3)]. The $I \propto V^2$ regime is often followed (with increasing applied voltage) by a sharp increase in the current corresponding to the filling of all the traps with injected carrier (trapped-filled limit), which, of course, is what we observe in our devices (Figs. 6 and 9). SCLC has been proposed as a mechanism to explain the electrical behavior of resistive memory devices; see, for example, Ref. 30. However, the expression for tunneling conductivity in Eq. (2) can also exhibit a current versus voltage behavior that seems to be of the form of $I \propto V^2$.[31]

The theory developed by Simmons and Verderber relies on a defect band in the insulator having a finite energy width and a particular energy relationship with the Fermi level in the metal. In the low conductivity (OFF) state, all the traps in the organic material are filled, while the ON state occurs when the trapping levels are empty. As the applied voltage in the NDR region is increased, the buildup of space charge in the traps reduces the current. Rapidly decreasing the voltage from that corresponding to the minimum current to zero turns the device OFF as this action leaves the trapping centers charged. On the other hand, if the device voltage is switched to zero from the value corresponding to the maximum current, the device state remains ON (traps uncharged). Our measurements show very little change in the device capacitance between its ON and OFF states, suggesting that there is little charge storage in the devices.

Neither of the models described above provides a completely satisfactory explanation for all of our experimental data. The metallic filamentary model is attractive in that it certainly accounts for the observation of switching and NDR in a wide range of thin film systems and explains the noisy

(and somewhat random) nature of the switching events observed by ourselves and others (see, for example, Fig. 15). However, the fact that our devices still work when an additional layer (Cr or a LB film) is interposed between the top electrode and the organic layer provides a strong argument against this theory.

Rozenberg *et al.* put forward a phenomenological model based on the assumption that the semiconducting part of the memory device possesses a nonpercolating domain structure, in particular, regions adjacent to the electrodes together with a central domain.[32] The electrical behavior is then characterized by domain-domain and domain-electrode tunneling rates and the number of domains. This idea may have some merit when applied to our devices. Although the development of a full model is beyond the scope of this experimentally based paper, we put forward a tentative explanation for our results.

First, we suggest that the operation of our devices is dependent on two types of domain, or region, between the Al electrodes: a region immediately adjacent to the electrodes, which can be affected by the electrode evaporation conditions, and a central domain, which is mainly responsible for the observed switching and NDR effects. Carrier transport is determined by tunneling between the surface and the central domains and by the conduction process within the domains.

For the as-deposited (unformed) films, the conductivity is controlled by carriers moving between trapping states located throughout the film; the outcome is the observation of Poole–Frenkel conductivity. The application of a large positive voltage to the top Al electrode results in the nucleation of a percolating conductive pathway throughout the central domain. This process may involve the local phase change (e.g., a local crystallization of amorphous regions of the organic film) and could be influenced by the polar nature (dipole moments of the various chemical groups) of the thin film; the presence of metallic nanoparticles will also play an important role. In this respect, the process may be similar to the electric field poling of a ferroelectric material. Very thin film structures do not exhibit NDR or switching simply because there is no significant central domain; i.e., the electrical behavior is dominated by the electrode regions. Following the device formation, a relatively high current flows and Ohmic conductivity is observed. However, as the applied voltage is increased further, the conductive pathway is ruptured through heat dissipation and the current is confined to the amorphous regions of the central domain; the device current then falls with increasing applied voltage (NDR).

If the voltage at the current maximum is rapidly reduced to zero, then the device ON state is formed as the organic thin film still contains a conductive pathway between the electrodes. In contrast, if the voltage corresponding to the current minimum is reduced to zero, the connections between the conductive regions have been broken and the device OFF state is measured. Increasing the voltage for the device in this OFF state does not, however, reveal the *I-V* characteristics of an unformed device (i.e., Poole–Frenkel conductivity) as a conductive nanocrystalline infrastructure remains within the film. The current voltage behavior will be determined by the amorphous regions between the ruptured nanocrystalline segments in the central domain. For example, carriers may tunnel from one nanocrystal to the next, accounting for the nonlinear *I-V* behavior observed in Figs. 7 and 11.

The essential feature of the model suggested here is that the ON-state current is carried by conductive nanocrystalline regions within the organic thin film rather than by metal filaments. As a consequence, some dependence of the device operation on the chemical composition of the organic thin film (and also on the nature of defects and impurities within the film), as noted in our previous work, is expected.[11] The theory relies on the ability of these crystalline regions to form under the application of a voltage, in a fashion similar to the metallic filament model of Dearnaley *et al.*[22] The detailed nature of the internal structure of our films is unclear and prompts a number of experiments. The electrical behavior of our thin films may simply reflect a transition from surface-dominated to bulk-controlled processes and may be a natural feature of all thin films of semi-insulating materials. This would account for the wide ranging reports of memory and NDR phenomena.

V. CONCLUSIONS

Switching and NDR have been observed in crossed bar devices based on Al/organic layer/Al architectures in which the organic layer was a spin-coated layer of 7-{4-[5-(4-*tert*-butylphenyl)-1,3,4-oxadiazol-2-yl]phenyl}-9,9-dihexyl-*N*,*N*-diphenyl-fluoren-2-amine. However, the thin film must be greater than 50 nm in thickness in order to observe these effects. The addition of gold nanoparticles (0.5 wt %) did not change the switching behavior; however, devices incorporating the nanoparticles showed more reproducible characteristics. In most cases, a forming process, in which a positive voltage was applied to the top Al electrode, was required before the NDR and switching were observed. Three different electrical conductivity mechanisms have been identified: Poole–Frenkel conductivity in unformed structures, linear current versus voltage characteristics for the ON state for formed devices, and superlinear current versus voltage behavior for the OFF state in formed devices. Models based on metallic filament formation and charge injection/storage do not account for all our experimental observation. We suggest that a domain structure in which charge transport can occur through nanocrystalline regions may provide a better explanation for our data. The development of a full model will be a subject of further work.

ACKNOWLEDGMENTS

This work was supported by The Engineering and Physical Sciences Research Council (EPSRC), the General Secretariat of Research and Technology, Greece, and the British Council, Greece. We would also like to thank Professor David L. Allara for useful discussions.

[1] K. Galatsis, Y. Wang, Y. Bostros, Y. Yang, Y.-H. Xie, J. F. Stoddart, R. B. Kaner, C. Ozkan, C. Zhou, and K. W. Kim, IEEE Circuits Devices Mag. **22**, 12 (2006).
[2] International Technology Roadmap for Semiconductors, 2005 (http://www.itrs.net/).

[3]J. C. Scott and L. D. Bozano, Adv. Mater. (Weinheim, Ger.) **19**, 1452 (2007).
[4]J. E. Green, J. W. Choi, A. Boukai, Y. Bunimovich, E. Johnston-Halperin, E. Delonno, Y. Luo, B. A. Sheriff, K. Xu, Y. S. Shin, H.-R. Tseng, J. F. Stoddart, and J. R. Heath, Nature (London) **445**, 414 (2007).
[5]L. D. Bozano, B. W. Kean, V. R. Deine, J. R. Salem, and J. C. Scott, Appl. Phys. Lett. **84**, 607 (2004).
[6]L. D. Bozano, B. W. Kean, M. Beinhoff, K. R. Carter, P. M. Rice, and J. C. Scott, Adv. Funct. Mater. **15**, 1933 (2005).
[7]Y. Yang, J. Ouyang, L. Ma, R. J.-H. Tseng, and C.-W. Chu, Adv. Funct. Mater. **16**, 1001 (2006).
[8]J. Chen and D. Ma, Appl. Phys. Lett. **87**, 023505 (2005).
[9]A. K. Mahapatro, R. Agrawal, and S. Ghosh, J. Appl. Phys. **96**, 3583 (2004).
[10]C. Pearson, K. Kamtekar, J. Ahn, C. Wang, M. R. Bryce, and M. C. Petty, UK Patent Application No. 0703864.9 (pending).
[11]C. Pearson, J. H. Ahn, M. F. Mabrook, D. Zeze, M. C. Petty, K. T. Kamtekar, C. Wang, M. R. Bryce, P. Dimitrakis, and D. Tsoukalas, Appl. Phys. Lett. **91**, 123506 (2007).
[12]K. T. Kamtekar, C. Wang, S. Bettington, A. S. Batsanov, I. F. Perepichka, M. R. Bryce, J. H. Ahn, M. Rabinal, and M. C. Petty, J. Mater. Chem. **16**, 3823 (2006).
[13]M. Green and P. O'Brien, Chem. Commun. (Cambridge) 2000.
[14]S. Paul, C. Pearson, A. Molloy, M. A. Cousins, M. Green, S. Kolliopoulou, P. Dimitrakis, P. Normand, D. Tsoukalas, and M. C. Petty, Nano Lett. **3**, 533 (2003).
[15]G. G. Roberts, N. Apsley, and R. W. Munn, Phys. Rep. **60**, 59 (1980).
[16]D. Braun, J. Polym. Sci., Part B: Polym. Phys. **41**, 2622 (2003).
[17]R. L. McCreery, Chem. Mater. **16**, 4477 (2004).
[18]R. Stratton, J. Phys. Chem. Solids **23**, 1177 (1962).
[19]M. Arif, M. Yun, S. Gangopadhyay, K. Ghosh, L. Fadiga, F. Galbrecht, U. Scherf, and S. Guha, Phys. Rev. B **75**, 195202 (2007).
[20]T. Ouisse andO. Stéphan, Org. Electron. **5**, 251 (2004).
[21]J. G. Simmons and R. R. Verderber, Proc. R. Soc. London, Ser. A **301**, 77 (1967).
[22]G. Dearnaley, D. V. Morgan, and A. M. Stoneham, J. Non-Cryst. Solids **4**, 593 (1970).
[23]G. Dearnaley, A. M. Stoneham, and D. V. Morgan, Rep. Prog. Phys. **33**, 1129 (1970).
[24]M. Cölle, M. Büchel, and D. M. De Leeuw, Org. Electron. **7**, 305 (2006).
[25]F. Verbakel, S. C. J. Meskers, R. A. J. Janseen, H. L. Gomes, M. Cölle, M. Büchel, and D. M. De Leeuw, Appl. Phys. Lett. **91**, 192103 (2007).
[26]G. L. Fisher, A. V. Walker, A. E. Hooper, T. B. Tighe, K. B. Bahnck, H. T. Skriba, M. D. Reinard, B. C. Haynie, R. L. Opila, N. Winograd, and D. L. Allara, J. Am. Chem. Soc. **124**, 5528 (2002).
[27]A. M. Walker, T. B. Tighe, O. M. Carbarcos, M. D. Reinard, B. C. Haynie, S. Uppili, N. Winograd, and D. L. Allara, J. Am. Chem. Soc. **126**, 3954 (2004).
[28]W. Tang, H. Shi, G. Xu, B. S. Ong, Z. D. Popovic, J. Deng, J. Zhao, and G. Rao, Adv. Mater. (Weinheim, Ger.) **17**, 2307 (2005).
[29]A. Mallikarjunan, S. P. Murarka, and T.-M. Lu, Appl. Phys. Lett. **79**, 1855 (2001).
[30]H. T. Lin, Z. Pei, and Y. J. Chan, IEEE Electron Device Lett. **28**, 569 (2007).
[31]M. Palumbo, K. U. Lee, B. T. Ahn, A. Suri, K. S. Coleman, D. Zeze, D. Wood, C. Pearson, and M. C. Petty, J. Phys. D **39**, 3077 (2006).
[32]M. J. Rozenberg, I. H. Inoue, and M. J. Sánchez, Phys. Rev. Lett. **92**, 178302 (2004).